

# Infrared study of the superconducting phase transition in $\text{YBa}_2\text{Cu}_3\text{O}_{7-x}$

D. van der Marel<sup>1</sup>, H.-U. Habermeier, D. Heitmann, W. König and A. Wittlin<sup>2</sup>

*Max-Planck-Institut für Festkörperforschung, Heisenbergstrasse 1, W-7000 Stuttgart 80, Germany*

Received 27 December 1990

Revised manuscript received 7 March 1991

We observe a critical behaviour near  $T_c$  in the infrared reflectivity of  $c$ -axis oriented  $\text{Y}_1\text{Ba}_2\text{Cu}_3\text{O}_{7-x}$  films prepared with pulsed in situ laser deposition. From an analysis of the temperature dependence of the spectra, which were measured with intervals of 5 K in a large temperature range around  $T_c$  we obtain (1) the temperature dependence of the superfluid fraction, and (2) the temperature dependence of the absorption edge at  $400\text{ cm}^{-1}$ . We show that the superfluid fraction follows closely a  $1 - (T/T_c)^4$  law. We show furthermore that the *height* of the absorption edge closely follows the behaviour of the superfluid fraction, whereas the energetic *position* of the edge is practically constant up to  $T_c$ . This behaviour can be understood in a semi-empirical way using a modified Gorter–Casimir two-fluid model using the concepts of a temperature independent gap and a temperature dependent density of the superconducting fraction. Above  $T_c$  we observe a dip in the self-energy of the dielectric function at the position of the absorption edge existing in the superconducting state.

## 1. Introduction

Since the discovery of cuprate high- $T_c$  superconductors by Bednorz and Müller [1] two major anomalies with respect to BCS theory directly connected to the superconducting state have been discussed: the oldest and best established one is the absence of a Hebel–Slichter [2] peak in the nuclear spin relaxation [3]. The second one has been the determination of the superconducting gap. A large variety of different gap values have been determined in the same materials using a variety of techniques. In particular the interpretation of the famous  $8k_B T_c$  edge structure that has been observed with infrared spectroscopy [4–8], energy loss spectroscopy [9], photoelectron spectroscopy [10] and tunneling [11] has been subject of many discussions and a wide va-

riety of explanations have been proposed. Very recently detailed measurements [12] of the temperature dependence of the frequency shift and relaxation rate of a large number of different phonon frequencies could be interpreted in connection with the formation of a superconducting gap that is slightly, but significantly, smaller than the  $8k_B T_c$  edge structure. There have been various observations of a much smaller gap-like feature in a number of samples [13]. In this paper we extend in great detail on an earlier indication [14,15] that in  $c$ -axis oriented high quality  $\text{Y}_1\text{Ba}_2\text{Cu}_3\text{O}_{7-x}$  samples there is only one feature in the range above  $100\text{ cm}^{-1}$  that can be identified as a gap. This is the  $8k_B T_c$  absorption edge. Although at low temperatures the spectral features can be well understood in terms of standard BCS theory, provided one accepts a distribution of  $\Delta$  between 200 and  $325\text{ cm}^{-1}$ , the temperature dependence of this feature has a totally new and anomalous phenomenology, i.e.  $\Delta$  itself does *not* depend on  $T$  in the temperature range of interest, but the superfluid fraction as well as the height of the edge follow closely a  $1 - (T/T_c)^4$  behaviour, which is also the temperature dependence of  $(\lambda(T)/\lambda(0))^2$ , where  $\lambda(T)$  is the

<sup>1</sup> Present address: Delft University of Technology, Faculty of Applied Physics, Lorentzweg 1, 2628 CJ Delft, The Netherlands.

<sup>2</sup> Also at Institute of Physics PAN PL, 02-668 Warszawa, Poland, research project RBPB 01.9. Present address: Katholieke Universiteit Nijmegen, Toernooiveld 1, 6525 ED Nijmegen, The Netherlands.

London penetration depth. Interestingly, Hebel and Slichter have made the following observation in their historical paper on nuclear spin relaxation in normal and superconducting aluminum [2]: “Reasonable assumptions for a two-fluid model would make the relaxation rate always slower in the superconductor (or in any event *either* always slower *or* always faster), so that nuclear spin relaxation does not seem capable of interpretation in terms of this theory”. One can reverse the argument in the case of the cuprate high- $T_c$  superconductors and argue that the absence of a Hebel–Slichter peak can be interpreted as an implication of two-fluid superconductivity of some kind. One has to bear in mind however, that the absence of a Hebel–Slichter peak can also be explained as a result of strong coupling [16], or anisotropy [17].

A detailed comparison of our data to model calculations based on BCS theory as well as an ad hoc two-fluid model with a constant value of  $\Delta$  for the superfluid fraction and a temperature-dependent superfluid fraction, very convincingly favours the latter model. This behaviour does not follow directly from strong coupling BCS theory. In addition and probably closely related to this we find indications for a small fraction of pairs above  $T_c$ , again characterised by this same energy of  $8k_B T_c$ . This can either be interpreted as non-gaussian superconducting fluctuations, or as a mixture in the normal state of single-charge carriers and local pairs, e.g. bipolarons. These normal-state anomalies and the anomalous temperature dependence of the gap seem to be intimately related and point in the direction of a thermodynamics that is neither described by Bose condensation of pre-existing pairs nor by BCS theory. In any case the persistence of a small fraction of material with the  $8k_B T_c$  edge above  $T_c$  is in conflict with a gap that closes at  $T_c$ .

## 2. Experimental

### 2.1. Sample preparation and characterisation

*c*-Axis oriented thin films with thicknesses between 2000 Å and 4000 Å were prepared using the pulsed laser deposition technique set up for in situ Y–Ba–Cu–O thin film growth. Experimental details

have been published elsewhere [18]. Characterisation of the films using scanning electron microscopy, optical microscopy, and X-ray diffraction revealed that the films are single phase and *c*-axis oriented with a smooth surface. The substrates are single crystals of SrTiO<sub>3</sub> and twinned crystals of LaAlO<sub>3</sub> ([100] surface) with a wedged backside. Transmission electron microscopic measurements demonstrated a well-defined substrate/film interface on an atomic scale.

In this paper we report on the reflectivity measured on two thin films of 300 nm on SrTiO<sub>3</sub> (sample A) and on LaAlO<sub>3</sub> (sample B). The motivation to use samples of limited thickness is, that the best quality and *c*-axis orientation is obtained for samples with a thickness of less than 400 nm. In fig. 1 we present the SQUID susceptibility measurements and the resistivity curves on these two samples. These measurements were done after all infrared measurements were completed. We see that both samples have a sharp superconducting transition between 89 K and 90 K. The resistivities at 300 K are approximately 200  $\mu\Omega$  cm and 400  $\mu\Omega$  cm for samples A and B.

### 2.2. Measurement procedures and data handling

Infrared measurements were carried out in the far infrared (FIR) range (60  $\text{cm}^{-1}$ –700  $\text{cm}^{-1}$ ) and middle infrared (MIR) range (450  $\text{cm}^{-1}$ –7000  $\text{cm}^{-1}$ ) using a Fourier transform spectrometer. The measurement procedure was as follows: Both spectral ranges were measured in separate sessions, in which we first measured a reference mirror (Al and

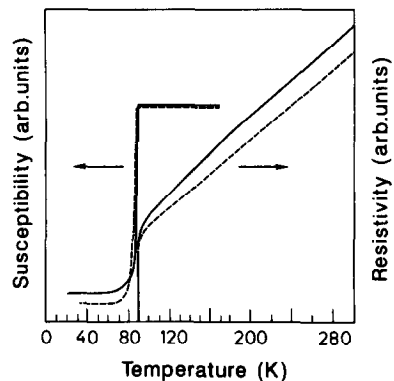


Fig. 1. DC SQUID susceptibility and resistivity of samples A (dashed curve) and B (solid curve).

Ag) at all temperatures, followed by a session in which the sample was measured at the same set of temperatures, and (not always) a third session in which again the mirror was measured at all temperatures. By comparing the results obtained on the mirror in two independent sessions we could estimate the effect of thermal drift and of the unavoidable slight differences in mounting of the sample and the mirror on the spectra. From accumulated experience we know that it is essential to repeat the sessions for the sample and the mirror in exactly the same way in order to get a reproducible result, with systematic errors of the absolute reflectivity smaller than 0.5%. To this end we stepped in regular intervals of 10 minutes and 5 K through the temperature region between 20 K and 150 K after an initial cool-down in larger steps of 50 K in all measurement sessions. The physical reason why this is important is that due to the long time constants in cooling of the substrate holder gradual changes in sample position take place during the whole measurement session, which influences the optical path. The MIR is more susceptible to this, and as a result the absolute accuracy we obtained in this range is only 3%, although the relative accuracy of the spectra taken at different temperatures during the same session is better than 0.5%. In the FIR both the absolute and the relative accuracy obtained is better than 0.5% if the correct procedure is followed.

The MIR spectra were joined to the FIR spectra using a scaling factor to overcome the 3% misfits in the regions of overlap. We took care here to use the *same* scaling factor for all temperatures measured, in order not to impose the measured temperature dependence in the FIR onto the MIR. For the present study where we concentrate on rather subtle temperature dependences in the FIR and in the MIR this is essential. Discontinuities of the order of 0.5% of the absolute reflectivity are then found at the frequency where the two spectral ranges are fitted together. In those cases where we wish to make a Kramers–Kronig analysis, a weighted average in the region of spectral overlap is used to join the spectral ranges smoothly. In the reflectivity spectra presented in this paper we only scaled the MIR to the FIR in the way described above. No additional scaling of the spectra was used, so that our estimate of the overall absolute accuracy is 0.5%. When comparing

the spectra taken at two subsequent temperatures we conclude that the relative accuracy on a limited temperature (and time) interval is better than 0.1%, but typically systematic deviations of 0.5% develop during the 4.5 hours it takes to cover the temperatures range between 20 K and 150 K.

### 3. Experimental results

#### 3.1. Reflectivity spectra

In figs. 2 and 3 we display the reflectivities of both samples as a function of frequency and temperature. In fig. 3(b) we also display the reflectivity of  $LaAlO_3$  together with a fitted theoretical curve using the expression.

$$\epsilon(\nu) = \epsilon_\infty + \sum_{j=1}^p \frac{S_j \nu_j^2}{\nu_j^2 - \nu^2 - i\nu\Gamma_j}.$$

In table 1 we give the fit parameters. On comparing the reflectivity with the substrate data we conclude that the peaks at 188, 429 and 670  $cm^{-1}$  in fig. 3 are due to substrate phonons. The wiggly structures between 700 and 900  $cm^{-1}$  in fig. 3 are of instrumental origin and depend on the accuracy with which the positioning of the sample and the mirror can be reproduced. The same holds for the small dip at 370  $cm^{-1}$  seen in the reflectivity data of sample A and B. This assignment is based on dividing the spectra of an Al mirror before and after slightly changing the alignment, where we found bumps at the same frequencies on an otherwise flat background. At 315  $cm^{-1}$  we observe a peak at the 1% level, which is not instrumental and which corresponds to the *c*-axis phonon which dominates the reflectivity spectra of ceramic samples and *ab*-oriented single crystals. In principle it is a forbidden transition in normal incidence spectra of *c*-axis oriented single crystals. Its weak presence in our spectra may be due to a relaxation of the optical selection rules due to small deviations from perfect stoichiometry.

Both in figs. 2 and 3 we observe the following important trend as a function of temperature: The reflectivity increases until an abrupt decrease sets in at  $T_c$  for frequencies above 600  $cm^{-1}$ , whereas for frequencies below 600  $cm^{-1}$  a sudden increase in reflectivity occurs, resulting in the development of a

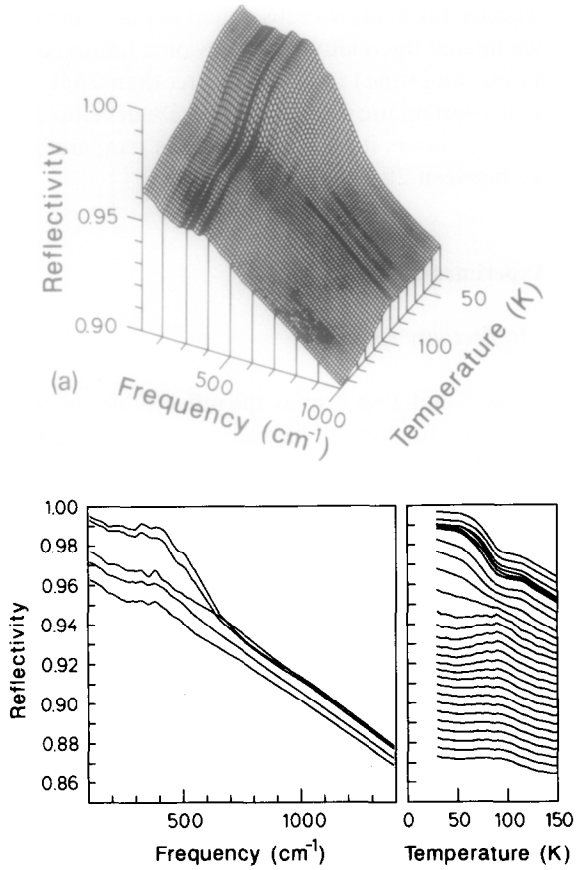


Fig. 2. Experimental reflectivity data of a  $c$ -axis oriented  $Y_1Ba_2Cu_3O_{7-x}$  film on a  $SrTiO_3$  substrate as a function of frequency and temperature. (a) 3D representation. (b) Left: Frequency dependence of the reflectivity measured at (from top to bottom):  $T = 30, 60, 90, 120,$  and  $150$  K. Right: Temperature dependence of the reflectivity measured at (from top to bottom)  $\nu = 100$   $cm^{-1}$ , to  $1450$   $cm^{-1}$  with increments of  $50$   $cm^{-1}$ .

pronounced shoulder at  $400$   $cm^{-1}$ . As the data corresponding to sample A show no peaks due to the substrate, we will study these features more closely using a Kramer–Kronig analysis. We will return to the reflectivity data corresponding to sample B as well as sample A when we compare the data to theoretically obtained reflectivity curves in the discussion.

### 3.2. Low frequency fit

In order to make a proper Kramers–Kronig analysis of the data we need extrapolations to the low- and high-frequency sides of the spectra which are physically meaningful. For  $T > T_c$  the sample is in the

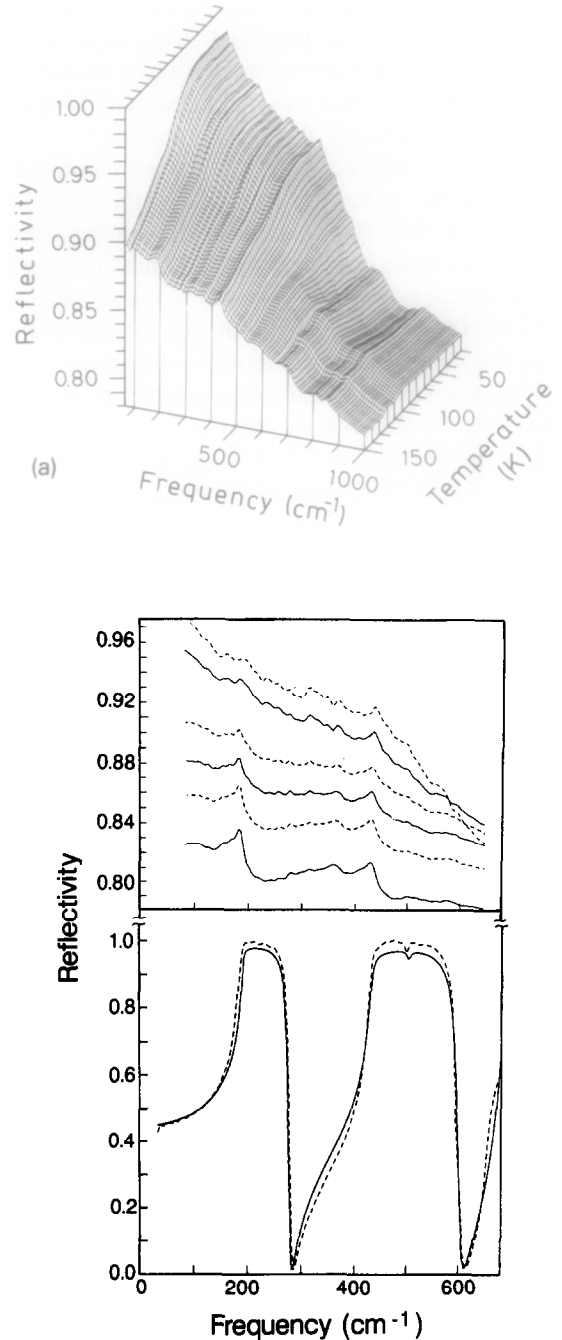


Fig. 3. Experimental reflectivity data of a  $c$ -axis oriented  $Y_1Ba_2Cu_3O_{7-x}$  film on a  $LaAlO_3$  substrate as a function of frequency and temperature. (a) 3D representation. (b) Top: Frequency dependence of the reflectivity measured at (from top to bottom):  $T = 35, 85, 135, 185, 235$  and  $285$  K. Bottom: Reflectivity of  $LaAlO_3$  (dashed) and a fitted spectrum (solid).

Table 1  
Optical constants for  $SrTiO_3$  [19] and  $LaAlO_3$

$j$	$\nu_j(\text{cm}^{-1})$	$S_j$	$\Gamma_j(\text{cm}^{-1})$
<b>LaAlO<sub>3</sub></b>			
	$\epsilon_\infty = 2.47$		
1	188	15.8	2.82
2	429	5.9	6.44
3	500	0.011	7.5
4	678	1.22	10.17
<b>SrTiO<sub>3</sub></b>			
	$\epsilon_\infty = 5.20$		
1	96	236	7
2	177	7	13
3	552	1.38	20

metallic state and the dielectric constant is well approximated by the Drude–Lorenz form in a limited frequency interval around the origin. The reflectivity can be well approximated by the Hagen–Rubens formula for frequencies much smaller than the scattering rate. In the superconducting state, for frequencies smaller than the gap, (1) the reflectivity need not be 100%, and (2) the Hagen–Rubens formula does not give the appropriate frequency dependence of the reflectivity. The appropriate form of the dielectric function for frequencies below the gap is

$$\epsilon(\nu) = \epsilon_\infty - \frac{\nu_s^2}{\nu(\nu + i0^+)} - \frac{\nu_p^2 - \nu_s^2}{\nu(\nu + i\Gamma)}. \quad (1)$$

If the charge-carrier density in the superconducting state and in the normal state is the same we can define a superfluid fraction

$$n_s(T) = (\nu_s(T)/\nu_p)^2. \quad (2)$$

This form is based on a Drude description of both the superfluid component (resulting in a  $\delta$ -function contribution to the conductivity) and of the normal component. In the BCS picture the normal component is formed by the thermally excited quasiparticles, that in principle only contribute at finite temperature (unless the gap has nodes). This form of the dielectric function has, however, a wider applicability as long as the optical response is dominated by a superfluid component and a damped Drude-like component. Note that the Drude form is a fairly good approximation to the metallic response which was derived independently of (and long before) the Fermi-liquid description of metals, which is in prin-

ciple equally applicable to non-Fermi liquid-like systems such as a gas of bosons. The reflectivity for small  $\nu$  than takes the form

$$R = 1 - \sqrt{\frac{\nu}{\nu_{HR}}} \sqrt{\frac{\nu(\sqrt{\nu^2 + \nu_X^2} - \nu_X)}{\nu^2 + \nu_X^2}}, \quad (3)$$

where

$$\nu_{HR} = \frac{\nu_p^2(1 - n_s)}{8\Gamma},$$

and

$$\nu_X = \frac{n_s\Gamma}{1 - n_s}.$$

For small values of  $n_s$ ,  $\nu_X$  converges to zero and we retain the Hagen–Rubens formula where  $1 - R$  scales with the square root of the frequency. For finite values of  $n_s$  there is a cross-over frequency  $\nu_X$  below which  $1 - R$  has the qualitatively different  $\nu^2$  behaviour and above which we retain the Hagen–Rubens form with a reduced plasma frequency. For  $n_s = 1$  the reflectivity is unit for all frequencies up to the gap frequency, where absorption across the gap sets in. For small  $n_s$  (i.e. near  $T_c$ ) the cross-over frequency  $\nu_X$  is approximately  $n_s(T)\Gamma$ , i.e. smaller than or of the order of the scattering rate, which in the case of the present samples amounts to a few hundred wavenumbers. We fitted our reflectivity data between 100 and 300  $\text{cm}^{-1}$  to the above dielectric function, where we added an additional temperature independent Drude oscillator  $\nu_{\min}^2 \nu^{-1} (\nu + i\Gamma_{\min})^{-1}$  which represents the contribution due to the chains [20]. In the least squares fit only  $n_s$  and  $\Gamma$  where varied. The other parameters are given in table 2. The motivation for this choice of parameters of the chain contribution will be discussed later in this paper, and corresponds

Table 2  
Drude parameters used for fitting theoretical curves to the reflectivity curves of samples A and B. All parameters except  $\epsilon_\infty$  are in  $\text{cm}^{-1}$ .

	Sample A	Sample B
$\nu_p$	11000	8000
$\Gamma$	fig. 5	$120\sqrt{(1 + (T(\text{K})/90)^2)}$
$\nu_{\text{mir}}$	17000	1800
$\Gamma_{\text{mir}}$	4500	4500
$\epsilon_\infty$	5.0	3.7

closely to the optical conductivity obtained for un-twinned single crystals [20]. The addition of this extra Drude term does not affect the values we find from the fit for  $n_s(T)$ , but has a considerable influence on the values found for  $\Gamma$ .

In fig. 4 we present the experimental curves together with the fits for a number of temperatures. The agreement is good with deviations of only 0.2%. Very clearly there is no indication in the experimental curves of a gap-like feature in this frequency regime. Nevertheless the fit to be Drude model in the normal state is very satisfactory, and the deviation of about 4% from perfect reflectivity in the normal state indicates that *if* a BCS gap would exist in this frequency regime, the superconductor would be sufficiently “dirty” to make it well observable. This is also borne out by our model calculations using generalized Mattis–Bardeen expressions covering the case of intermediate “cleanliness”, which we will present in the discussion section. It has been postulated earlier, that the superconducting cuprates might be too “clean” to have an observable effect on the reflectivity due to the opening of a gap [8]. The weak wiggles in the experimental curves are of the order of magnitude of the instrumental precision and will not be discussed. In fig. 5 we display the temperature dependence of  $n_s(T)$  (full circles) and  $\Gamma$  obtained from this least-squares fit. We see that there is a distinct temperature dependence with an abrupt change at  $T_c$ . Above  $T_c$  we find that  $n_s(T)$  is almost zero; the remaining small deviation from zero falls within the 0.5% experimental uncertainty in the absolute re-

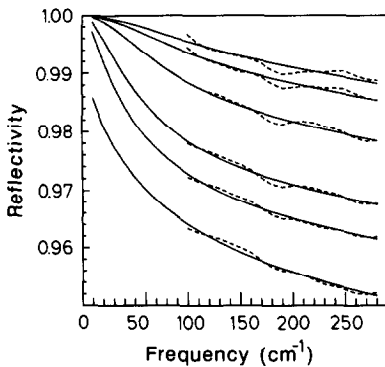


Fig. 4. Experimental reflectivity of sample A (dashed curves) together with a theoretical fit in the low-frequency region (solid curves). From top to bottom:  $T = 30, 60, 75, 90, 120,$  and  $150$  K.

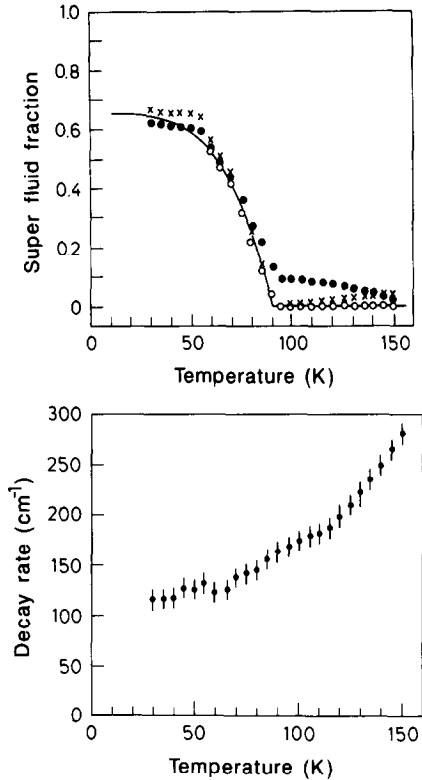


Fig. 5. (a) Solid curve:  $1 - (T/T_c)^4$ , closed circles:  $n_s$  obtained from fit with  $\Gamma$  and  $n_s$  as parameters, open circles: adjusted values of  $n_s$ , crosses:  $n_s$  obtained from integrating the conductivity. (b)  $\Gamma$  obtained from fit with  $\Gamma$  and  $n_s$  as parameters.

fectivity. We know that the resistivity above  $T_c$  is almost linear, hence the deviations from linearity are also related to systematic errors in the determination of the absolute reflectivity. As we want to avoid the use of extrapolations which are physically meaningless, we deliberately set  $n_s(T) = 0$  above  $T_c$  and slightly rescale the values below  $T_c$  (open circles) in our Kramers–Kronig analysis. The extrapolations of the reflectivity curves are then made with these values of  $n_s(T)$  and with  $\Gamma$  as the only fit parameter.

The temperature dependence of  $n_s$  closely follows a  $1 - (T/T_c)^4$  law, and is essentially temperature independent below 50 K. A second important observation at this point is that in our samples apparently not all spectral weight of the Drude response function collapses into a  $\delta$ -function. This is already directly evident from the reflectivity spectra, which do not reach 100%, even at the lowest temperatures.

There is a number of possible explanations for this rather unexpected behaviour: In writing eq. (1) we implicitly assumed that we are in a frequency range below the BCS gap (if there is any). If the component described by the damped Drude oscillator has a BCS-like energy gap sufficiently far below  $100\text{ cm}^{-1}$  we would not notice the influence of this although  $n_s(T)$  could still be 100% at low temperatures. The second possibility is that our samples contain about 35% of metallic nonsuperconducting phases. The unlikely thing about this is that a concentration of 35% would not escape detection by X-ray diffraction or electron microscopy, which has been used to characterise our samples. One could speculate that such metallic phases exist in near-stoichiometric  $YBaCuO$  (1:2:3:7) without changing the lattice structure. The observation of a normal metallic component in the dielectric response is in accord with the observation of the linear term in the specific heat at low temperatures, the weight of which is a strongly sample-dependent property. Loram et al. and Phillips et al. [21,45] recently found about 10% of the normal-state free-electron contribution at  $T \ll T_c$  for undoped samples ranging to more than 90% for samples where 10% of the copper atoms have been replaced by Zn.

The temperature dependence of  $\Gamma$  (fig. 5) reflects the linear temperature dependence of the normal-state reflectivity. The deviations of perfect linear behaviour above  $T_c$  reflect systematic errors in the reflectivity of about 0.2% which we discussed in the previous section. If we extrapolate the Drude expression eq. (1) to zero frequency we obtain a DC resistivity at 100 K of about  $75\ \mu\Omega\text{ cm}$ . This value is consistent with the DC conductivity in the  $ab$ -plane [23] measured on good single crystals. There are two different ways to obtain an estimate for the effective mass of the charge carriers at this point. Either one extracts an effective mass from the plasmon frequency, assuming a value for the density of charge carriers, or one combines our value for the decay rate  $\Gamma$  with the mobility extracted from experimental Hall and resistivity data, in both cases using Drude expressions. As our extrapolated value of the DC resistivity corresponds to the value found using transport measurements both types of analyses automatically results in the same estimate of the effective mass. The in-plane Hall coefficient is temperature

dependent [24] and corresponds to an effective carrier density of  $3 \times 10^{21}\text{ cm}^{-3}$  at 100 K and  $9 \times 10^{21}\text{ cm}^{-3}$  at 300 K. Using the Drude expression for the plasma frequency ( $11000\text{ cm}^{-1}$ , see table 2) one obtains a temperature dependent mass ranging from  $2.2m_e$  at 100 K to  $6.7m_e$  at 300 K.

### 3.3. Optical conductivity

In fig. 6 we display the conductivity obtained from a Kramers–Kronig transformation of our data for a number of temperatures. We used the low-energy extrapolation discussed in the previous section below  $100\text{ cm}^{-1}$  and a high-energy extrapolation using two Drude terms with a frequency independent decay rate. For frequencies above  $30\,000\text{ cm}^{-1}$  a constant value for the dielectric constant was assumed. On comparing this with a Kramers–Kronig transform using an extrapolation where we assumed a decay rate that depends linearly on frequency we find no noticeable differences for our frequency range of interest, i.e. below  $2000\text{ cm}^{-1}$ . Our data agree well with earlier published data, except for frequencies below about  $250\text{ cm}^{-1}$  where some authors have claimed to find a BCS-like gap. Whether or not this gap has really been observed is debatable, basically because there is usually a rather large systematic experimental error in the absolute value of the measured reflectivity, as has recently been pointed out by Orenstein et al. [6]. In the case of our data we are confident that there is no gap observable in this frequency range, in the first place because of the good fit obtained in fig. 4 and in the second place because

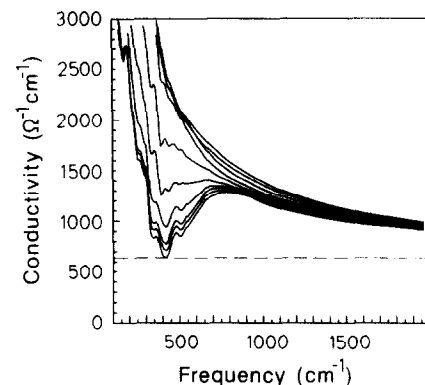


Fig. 6. Optical conductivity of sample A. From bottom to top:  $T = 30\text{ K}$  to  $150\text{ K}$  with increments of  $10\text{ K}$ .

we observe no temperature dependent step as one would expect. Taking the scattering rate of fig. 5 of about  $120 \text{ cm}^{-1}$  and assuming that  $2\Delta$  is somewhere between  $100$  and  $300 \text{ cm}^{-1}$  we obtain a value for  $\Gamma/(2\Delta)$  between  $0.4$  and  $1.2$ , which would result in a drop in reflectivity of about  $3\%$  at  $h\nu=2\Delta$ . Whether or not one assumes that such a gap exists has negligible influence on the conductivity above the assumed gap value after Kramers–Kronig transformation of the reflectivity, but it has a considerable influence on the integrated spectral weight.

The dashed curve in fig. 6 corresponds to the contribution of the chain conductivity of table 2. On comparing with published data on untwinned single crystals with fig. 6 we found that the chain contribution [20] is well represented by the Drude parameters of table 2. In the subsequent analysis we will subtract this part from the conductivity. In fig. 7 we display the conductivity relative to the normal-state conductivity, where we subtracted the dashed curve of fig. 6. The subtraction does not influence the position of the various features, but stretches the scale by about  $20\%$ . In order to prevent the figure from becoming cluttered we only display the curves below  $T_c$  here. The data are clearly dominated by an absorption edge which rises steeply between  $400$  and  $800 \text{ cm}^{-1}$ . Above  $T_c$  the edge in the conductivity cannot be discerned directly. The curves normalized to the  $95 \text{ K}$  conductivity still show an inverted structure at the same position, which is however an order of magnitude weaker.

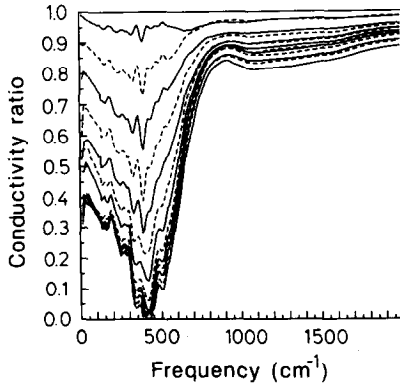


Fig. 7. Optical conductivity of sample A scaled to the conductivity at  $95 \text{ K}$ . From bottom to top:  $T=30 \text{ K}$  to  $90 \text{ K}$  with increments of  $5 \text{ K}$ .

### 3.4. Frequency-dependent decay rate and mass

In order to amplify these rather small features above  $T_c$  we determine the frequency dependent decay rate  $\gamma(\nu)$  and effective mass  $m^*(\nu)$  defined by the relation:

$$\epsilon(\nu) = \epsilon_\infty - \frac{\nu_p^2 m / m^*(\nu)}{\nu(\nu + i\gamma(\nu))},$$

where  $\gamma(\nu)$  and  $m^*(\nu)$  are real numbers. Inversion of this relation allows us to express  $\gamma(\nu)$  and  $m^*(\nu)$  in terms of the experimental complex dielectric function:

$$\gamma(\nu) = -\nu \frac{\Im(\epsilon_\infty - \epsilon(\nu))}{\Re(\epsilon_\infty - \epsilon(\nu))},$$

$$m^*(\nu)/m = \Re \frac{(\nu_p/\nu)^2}{\epsilon_\infty - \epsilon(\nu)}.$$

For  $\epsilon_\infty$  and  $\nu_p$  we use again the values of table 2. Alternatively one can write the dielectric constant in the following form:

$$\epsilon(\nu) = \epsilon_\infty - \frac{\nu_p^2}{\nu(\nu + \Sigma(\nu))},$$

$$\Sigma(\nu) = \frac{m^*(\nu)}{m} (\nu + i\gamma(\nu)) - \nu,$$

where  $\Sigma$  is a frequency-dependent self-energy obeying Kramers–Kronig relations. In fig. 8 we present  $\gamma$  and  $m^*/m$  as solid curves for  $T > T_c$ , where we used the values of table 2 for  $\epsilon_\infty$  and  $\nu_p$ . In order to demonstrate that the dip in the decay rate occurs at the same energy position below and above  $T_c$  and furthermore coincides with the position of the absorption edge in the superconducting state we apply the same formula below  $T_c$ , resulting in the dashed curves. We have to warn here that in the superconducting state the values of the inverse lifetime thus obtained are physically meaningless. In an extensive study of a large number of different samples it has been established by Orenstein et al. [6] that the edge is a very generic materials property and persists in samples with lower doping and with a lower  $T_c$ . This led these authors to the suggestion that the threshold could be a charge-density wave gap. In thermopower often an anomalously sharp peak has been seen in several samples below  $150 \text{ K}$  [26]. This could be as-

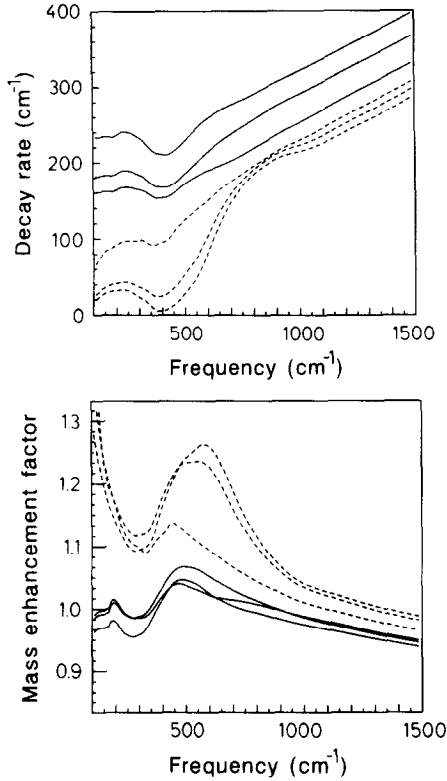


Fig. 8. Scattering rate and mass enhancement of sample A. From top to bottom (a) and from bottom to top (b):  $T = 150, 120, 90, 75, 60$  and  $30$  K. Solid curves:  $T \geq T_c$ , dashed curves  $T < T_c$ .

sociated with the formation of pre-existing pairs [27].

### 3.5. Energy loss and infrared transmission

Prior to discussing the physical implications of the results obtained by infrared reflectivity we first demonstrate that these are in line with observations with other techniques. We compare our results with recent high-resolution energy loss (HREELS) data and with infrared transmission of micro-cleaved single crystals. First we generate the energy loss function  $-\Im(1/\epsilon)$  from our experimentally determined dielectric function. We use the same representation as Demuth et al. [9], i.e. the ratios with respect to the loss function determined at  $T = 125$  K. In order to facilitate comparison to the HREELS data we use meV instead of  $\text{cm}^{-1}$  on the energy axis. The result is displayed in fig. 9 together with the experimental

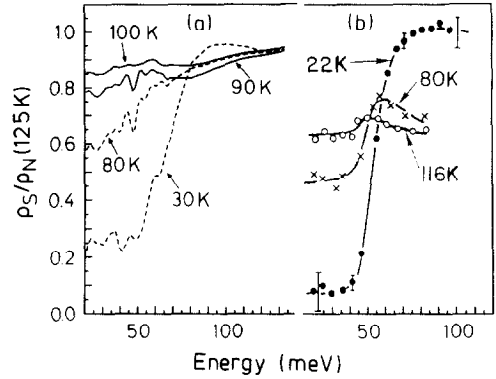


Fig. 9. (a) Loss function of sample A relative to 125 K. Temperatures are indicated. (b) Experimental loss function of  $Y_1Ba_2Cu_3O_4$  [9].

plot by Demuth et al. [9]. We see that there is good general agreement, including the presence of the tiny bump at around 50 meV that persists above  $T_c$ . The main difference is that in the curves generated from infrared reflectivity, the edge below  $T_c$  as well as the dip above  $T_c$  are broadened with respect to the experimental HREELS data. The reason for this is not clear, but it might be related to the higher sensitivity to surface conditions in HREELS.

The comparison to transmission spectra can be made by using the Fresnel formula for the normal transmission through a dielectric slab,

$$T = \left| \cos(nkd) - i \sin(nkd) \frac{1 + \epsilon}{2n} \right|^{-2},$$

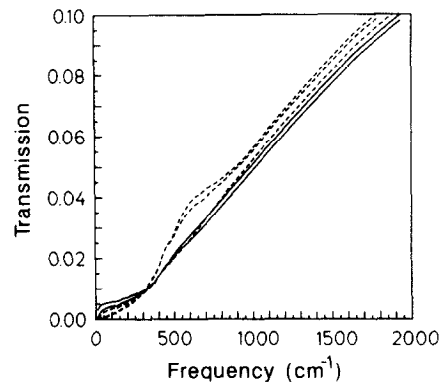


Fig. 10. Transmission through a slab of 100 nm thickness calculated from the experimentally determined dielectric function of sample A.

where  $n = \sqrt{\epsilon}$  is the complex optical constant of the sample material,  $d$  is the thickness of the slab and  $k = \omega/c$  is the wavevector of the light in vacuum. In fig. 10 we display the result for an unsupported thin film of 100 nm thickness, again using our experimentally determined dielectric constant. There is a striking similarity between this plot and recent results on  $Bi_2Sr_2CaCu_2O_8$  superconducting films [25]. We also see from these plots, that the feature at  $400 \text{ cm}^{-1}$  is not very pronounced in the superconducting state. Similar to the experimental results in transmission we see that the transmitted signal nowhere becomes zero, as should happen for a single-phase superconductor which has no normal Drude-like component contributing to absorption below the gap. Our result demonstrates that, although there is no clear feature in the transmission spectra that can be associated with an absorption threshold, one cannot conclude from this that there is no threshold feature in the dielectric function. In this case the absorption edge, which is very pronounced in the reflectivity, the conductivity and the loss functions, is removed from the transmission spectrum due to the combined effect of reflection/refraction and the presence of a rather strong normal component below the absorption threshold. The special point in the transmission spectra is the maximum at  $600 \text{ cm}^{-1}$ , which coincides with the midpoint of the absorption edge in the conductivity.

## 4. Discussion

### 4.1. Superfluid density

Before turning to the interpretation of the absorption threshold at  $400 \text{ cm}^{-1}$  we first consider again the results for the superfluid density. We already obtained the superfluid density from fitting the low-frequency part of the spectra, as displayed in fig. 5. We now study the same feature by comparing the integrated conductivity in the normal and in the superconducting state. In fig. 11 we display the function

$$N_{\text{eff}}(\nu) \equiv \frac{4m_e V_{\text{unit}}}{e^2} \int_{0^+}^{\nu} \sigma(\nu') d\nu',$$

using the notation of Orenstein et al. [6], i.e.  $m_e$  and

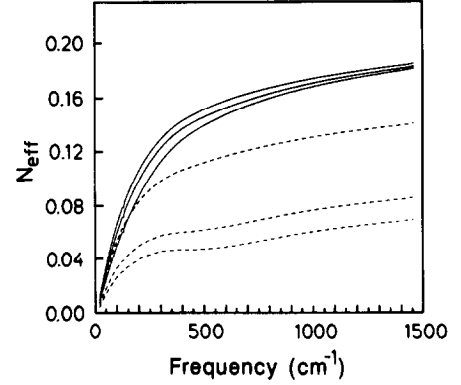


Fig. 11. Effective number of charge carriers per unit cell calculated from integrating the conductivity of sample A. From top to bottom:  $T = 150, 120, 90, 75, 60$  and  $30 \text{ K}$ .

$e$  are the bare electron mass and charge and  $V_{\text{unit}}$  is the unit cell volume. The number of charge per unit cell can be derived from  $N_{\text{eff}}$  by multiplying it with the relative effective mass. As there is no frequency where  $N_{\text{eff}}$  saturates, one cannot make an unequivocal assignment of the effective mass given a certain assumption for the density of charge carriers. If we assume that the density of charge carriers corresponds to about one hole per unit cell we can estimate that the effective mass is approximately  $4m_e$  (i.e. assuming that the charge carriers have charge  $e$ . If one assumes a charge of  $2e$  such as for bipolarons [40] one arrives at an effective mass of  $8m_e$  for the pairs.) Again a temperature independent ‘‘chain conductivity’’ has been subtracted from the conductivity, which influences the plot only slightly due to the low value of this broad Drude oscillator. The difference between  $N_{\text{eff}}$  in the normal state and in the superconducting state reflects the oscillator strength of the  $\delta$ -function corresponding to the superfluid component. This value must be determined at a frequency above the point where the difference saturates, which is in our case above  $700 \text{ cm}^{-1}$ . The contribution of the superfluid component to the optical conductivity is then:

$$\sigma_s(\nu) = \frac{\nu_s^2/2}{i\nu - 0^+},$$

where

$$\nu_s^2 = N_{\text{eff}} e^2 (\pi V_{\text{unit}} m_e)^{-1}.$$

The superfluid fraction is

$$n_s(T) = (\nu_s / \nu_p)^2$$

There is some arbitrariness in defining a proper value of  $\nu_p$ . We used the value of table 2, resulting in the crosses in fig. 5. The good agreement between  $n_s$  obtained from the low frequency fit and the latter analysis based on integration of the optical conductivity indicates that our analysis is internally consistent. The fact that the oscillator strength of the superfluid component is built up from contributions in the frequency region up to about  $400 \text{ cm}^{-1}$  with no contribution from the region above  $700 \text{ cm}^{-1}$ , indicates a close relationship between the  $400 \text{ cm}^{-1}$  absorption edge and superconductivity.

#### 4.2. Absorption edge

The nature of the absorption edge is subject of a continuing debate. In view of the fact that this structure almost completely disappears above  $T_c$  one is tempted to relate it to a BCS-like energy gap. Such an assignment has been advocated especially by Collins, Schlesinger and co-workers. As has been pointed out by the same authors in later publications [5], one of the difficulties with this interpretation is, that the structure shows almost no shift in position as a function of temperature.

The temperature dependence of the height of the edge as displayed in fig. 6 rules out another assignment [28] of the feature as an interference effect between a bound electronic band centered at  $400 \text{ cm}^{-1}$  and a phonon at  $433 \text{ cm}^{-1}$ , as there is no reason for this particular way in which the height of the feature depends on temperature unless as additional set of assumptions is made.

Another school of thought relates the absorption edge to a Holstein process [29,30]. As has been pointed out by a number of authors this is also not a likely assignment for the simple reason that in that case the position of the edge should also be temperature dependent, although the edge no longer shifts to zero frequency at  $T_c$ , but to the frequency of the Holstein phonon. If we take the data of fig. 12 this would lead to a gap value of less than  $50 \text{ cm}^{-1}$ , and it does not explain the presence of a precursor at the same energy above  $T_c$ .

The same problem arises if we assume that the feature is a strong coupling BCS-like gap that closes ab-

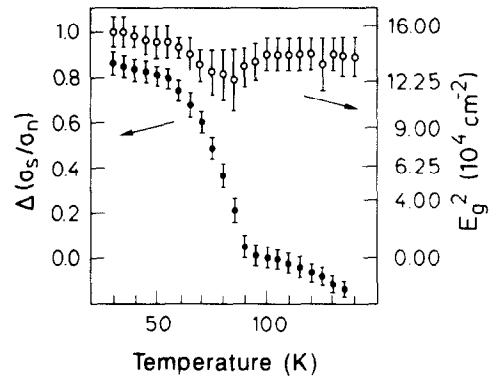


Fig. 12. Height of the edge in the relative conductivity of fig. 7 and the squared energy position of the edge.

ruptly close to  $T_c$  due to strong pair-breaking. Recent calculations of this type [31] successfully explain the absence of a Hebel-Slichter peak in the Korringa relaxation rate, basically due to strong smearing of the coherence peak in the quasi-particle density of states, and also predict a rather abrupt collapse of the gap near the transition temperature. Nevertheless the calculations predict a shift of the gap feature of about 30% already 10 K below  $T_c$ , and again it does not explain the precursor above  $T_c$ . We will discuss below that such an assumption also leads to strong disagreements with the experimentally determined temperature dependence of the reflectivity.

In fig. 12 we display both the squared energy position of this structure and the relative height as function of temperature, which is the central result of this paper. In weak and strong coupling versions of BCS theory  $|\Delta|^2$  is proportional to the order parameter close to  $T_c$ , which converges linearly to zero for  $T \rightarrow T_c$ . Surprisingly we see, that the *height* of the step, and *not* the squared energetic position follows this behaviour. The behaviour of the height of the step appears to be proportional to the superfluid fraction of fig. 5. This further establishes the close connection of the absorption edge to superconductivity. Although from the temperature dependence and from the presence of a damped Drude-like term below  $400 \text{ cm}^{-1}$  at low temperatures it seems to be unlikely that the edge is BCS energy gap in the usual sense, we first check whether at least the spectral shape obtained from BCS theory can be compared to the experimentally determined absorption edge. Our value of  $2\Delta$  is about  $80 \text{ cm}^{-1}$  higher than recent val-

ues based on interference between  $2\Delta$  and phonons measured with Raman spectroscopy [12]. This is a significant difference which is too large to be attributable to experimental inaccuracy. We give two possible reasons for the discrepancy:

(1) the phonons investigated with Raman spectroscopy may couple to only a relatively small part of the Fermi surface that contributes only little to infrared reflectivity. With infrared reflectivity one probes a weighted average over the whole Fermi surface, which in principle results in a distribution of gap values different from what is measured through the phonon shifts.

(2) The gap determined from the phonon shifts is a lower bound of a wide distribution of Holstein processes pinned to the electronic gap. With infrared spectroscopy one again observes the whole distribution, which then would show up at a higher frequency compared to the pure electronic gap. It is perhaps illuminating to point out that the absence of a temperature dependent shift of the edge is no longer in conflict with the interpretation as a Holstein process if we consider the gap-filling rather than gap-closing behaviour studied in this paper. The insensitivity to temperature and doping [6] of the frequency of the edge can even be extended to the insulating parents of the superconductors, where a similar absorption band is observed with photoexcited infrared spectroscopy [32].

### 4.3. Synthetic spectra

#### 4.3.1. $Y_1Ba_2Cu_3O_{7-x}$ on $SrTiO_3$

First we consider the conductivity function at essentially  $T=0$ . To that extent we use a generalized Mattis–Bardeen expression [33] for the dielectric response function of a superconductor with a finite electronic scattering rate. This formalism extends the early work by Mattis and Bardeen [34] (dirty limit) and by Leplae [35] (clean limit) and satisfactorily covers the whole range including both limiting cases. The formalism expresses the superconducting-to-normal conductivity ratio as a function of  $\nu/\Delta$ ,  $\tau\Delta$ , and  $T/\Delta$ . The conductivity in the superconducting state is obtained by multiplying with the normal-state conductivity determined by  $\nu_p$  and  $\tau$ . For the normal-state conductivity we assume a frequency and temperature dependent scattering rate given by the

following expression:

$$\tau^{-1} = 0.61 \sqrt{(\omega^2 + \pi(k_B T/\hbar)^2)}.$$

For the plasma frequency we adopted the value  $\nu_p = 9638 \text{ cm}^{-1}$ . For  $\Delta$  we assume a value of  $200 \text{ cm}^{-1}$ . To facilitate comparison the dashed curve of fig. 6 corresponding to the chain response was added. The result is the curve corresponding to the lowest temperature in fig. 13(a). The most important conclusion from comparing this plot to our experimental fig. 6 is that *if* there would be a BCS gap at around  $400 \text{ cm}^{-1}$  it would result in a step in the conductivity *with the same height and with roughly the same shape as the experimentally observed absorption edge*. Note that there is no freedom of parameters in the generalized Mattis–Bardeen expression allowing one to alter the shape of the edge once the normal-state conductivity is fixed by the scattering rate and the plasma frequency. The shape of the edge can only be improved in comparison to experiment if we assume a uniform distribution of  $2\Delta$  between  $400$  and about  $650 \text{ cm}^{-1}$ . The result is the curve corresponding to the lowest temperature on fig. 13(b), which now looks very similar to the corresponding curve in the experimental plot. A distribution of gaps can occur due to the very strong anisotropy of the Fermi surface, as has been stressed by Schneider et al. [36] and by Kresin and Wolf [37]. In principle the generalized Mattis–Bardeen expressions have to be adopted to anisotropic Fermi surfaces. It cannot be excluded that within the context of such a generalization of the formalism a better agreement of the spectral shape would be obtained without invoking a  $k$ -dependent gap function.

Let us now consider the temperature dependence of the conductivity curves. For the sake of comparison we assume a temperature independent gap and a temperature dependent weight factor  $f_s(T) = 1 - (T/T_c)^4$  in the optical response function corresponding to the experimental results displayed in fig. 12. We therefore have to introduce in an ad hoc manner the dielectric function

$$\epsilon = f_s(T)\epsilon_s + (1 - f_s(T))\epsilon_n,$$

which corresponds to a two-fluid model similar to the Gorte–Casimir model [39], with the modification that the superconducting fraction now has a gap as in BCS theory. The most important difference with

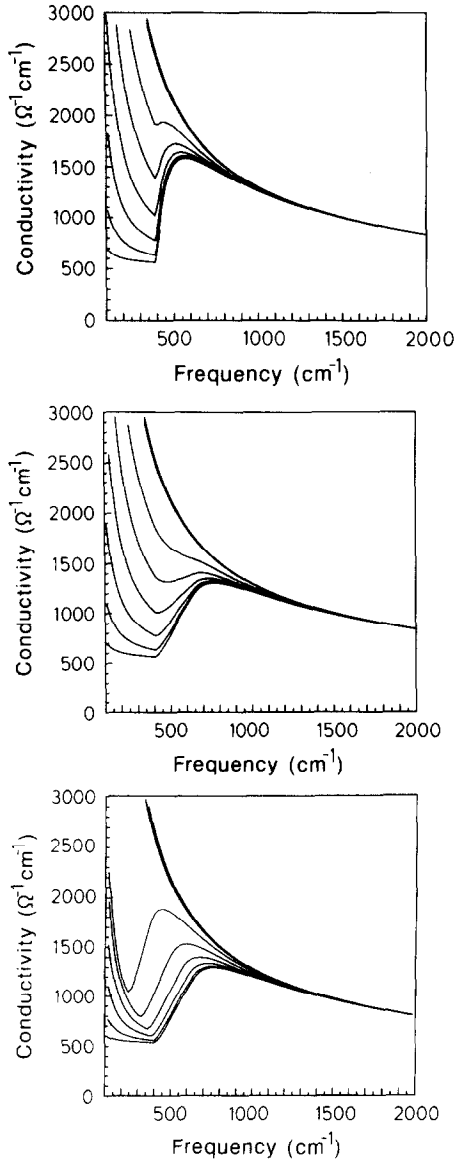


Fig. 13. Calculated conductivity using the ad hoc two-fluid model (a) with  $\Delta=200 \text{ cm}^{-1}$ , (b) with a distribution of  $\Delta$  between 200 and  $325 \text{ cm}^{-1}$ , (c) calculated conductivity using the BCS model. The temperatures are the same as in fig. 6.

BCS theory that we introduce here is that we assume that  $\Delta$  of the superconducting component behaves temperature independent. The dielectric function of the superconducting component is calculated with the parameters (except temperature, which has however little influence due to the large gap value) introduced above, with  $\Delta=200 \text{ cm}^{-1}$  at all tempera-

tures. We use the same parameters for  $\epsilon_n$  with  $\Delta=0$ . The resulting curves are displayed in figs. 13(a) and (b). Especially the latter set of curves looks very similar to the experimental set of curves of fig. 6.

For comparison we repeat the same analysis, now using the generalized Mattis–Bardeen expressions at finite temperature [33], which are based on weak-coupling BCS theory. This corresponds to having  $f_s=1$  at all temperatures, with a temperature dependent gap. We use the same uniform distribution of gaps as in fig. 13(b). For the temperature dependence we use

$$\Delta(T) = \Delta(0) \sqrt{\cos(0.5\pi(T/T_c)^\alpha)} \quad (4)$$

with  $\alpha=2$ , which is a good approximation for the temperature dependence of the gap in the weak coupling limit. The result is displayed in fig. 13(c). We see, that there are two significant differences:

- (1) the position of the edge is now temperature dependent, and
- (2) the height of the edge remains rather high up to temperatures close to  $T_c$ , in strong contrast with the experimental curves in fig. 6 and the behaviour displayed in fig. 12.

#### 4.3.2. $Y_1Ba_2Cu_3O_{7-x}$ on $LaAlO_3$

We also applied this type of analysis to the reflectivity of sample B. As we have to include multiple reflection between the film surface and the substrate here, a Kramers–Kronig analysis does not lead to meaningful results and we therefore calculate the reflectivity function which we then compare to the measured curves. The parameters used are a temperature-independent bulk plasma frequency and a temperature-dependent relaxation time ( $\tau$  proportional to  $1/T$ , with a saturation at about 60 K; the parameters are obtained from analysing single crystals in Bauer's Ph. D. thesis [38]). In addition we add a wide oscillator corresponding to a mid-infrared band. These parameters are also taken from the same single crystal analysis. All parameters are tabulated in table 2. Good agreement was obtained if we assume that in the superconducting state there is a normal component of 50%, i.e. we use  $f_s=0.5 \times (1 - (T/T_c)^4)$ . For  $\Delta$  we use the same temperature-independent distribution as in fig. 13(b). The dielectric functions of the substrate material and of the superconducting films were inserted in the ap-

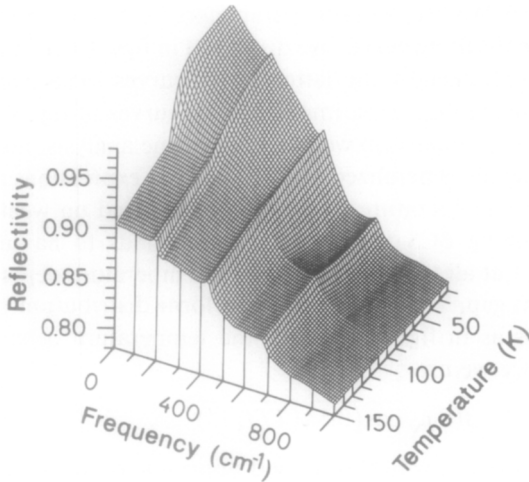


Fig. 14. Theoretical 3D plot corresponding to the reflectivity of sample B.

appropriate Fresnel formula for the combined substrate–thin film system:

$$r = \left| \frac{1 - n_{\text{eff}}}{1 + n_{\text{eff}}} \right|^2,$$

$$n_{\text{eff}} = n \frac{n_{\text{sb}} - i n \tan nkd}{n - i n_{\text{sb}} \tan nkd},$$

where  $n_{\text{sb}}$  is the dielectric constant of the substrate, resulting in the theoretical plot of fig. 14. We see that there is good overall agreement between figs. 14 and 3. To check the temperature dependence somewhat closer we compare in fig. 15(c) for a number of different frequencies the temperature dependences of

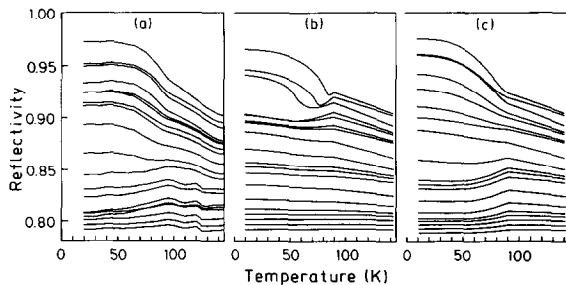


Fig. 15. (a) Experimental reflectivity data of sample B as a function of temperature for various values of the light frequency. (b) Theoretical reflectivity using BCS theory. (c) Theoretical reflectivity using the two-fluid model. From top to bottom:  $\nu = 100$  to  $1000 \text{ cm}^{-1}$  with increments of  $50 \text{ cm}^{-1}$ .

the reflectivity for the above model with the experimental data (fig. 15(a)). Again we see that agreement is satisfactory.

It is also interesting now to make a similar plot based on the BCS model using eq. (4) with  $\alpha = 2$ . This result is displayed in fig. 15(b). We clearly recognize a step at  $T_c$  in the low-frequency region, which shifts to lower temperatures as the frequency approaches  $2\Delta_0$ . Also there is a negative dip below  $T_c$  for frequencies below  $2\Delta$ , which is caused by the negative dipping of the reflectivity just above  $2\Delta$ : On approaching  $T_c$  from below,  $2\Delta(T)$  decreases. As soon as it becomes smaller than  $\nu$  the negative dipping sets in. This behaviour is manifestly absent in the experimental data of fig. 2(a). The disagreement with fig. 2(a) becomes stronger if we assume an energy gap of  $400 \text{ cm}^{-1}$  with a steeper temperature-dependent drop of the gap near  $T_c$  (we tried  $\alpha = 4$  and  $\alpha = 10$ ) which is more typical of strong-coupling theory: At low frequencies the reflectivity drops much too steeply with such an assumption, and the negative dipping does not disappear, but is squeezed in a narrower temperature interval. In the extreme case where we assume that  $\alpha \rightarrow \infty$ ,  $\Delta(T)$  becomes a step function. For frequencies below the energy gap the reflectivity then drops discontinuously at  $T_c$ , which is in strong disagreement with the observed behaviour in any of our samples. This the second reason why mean-field implementations of strong-coupling theory do not fit our results very well. The first reason mentioned above is the observation of a precursor of the absorption edge above  $T_c$ .

Note, that although at  $T=0$  we can fit our results very well to the generalized Mattis–Bardeen expressions [33], which could be taken as an indication that BCS theory holds, the behaviour of  $f_s$  and  $\Delta$  at finite temperature are in strong contrast with BCS theory: In BCS theory  $f_s$  (which is *not* the superfluid fraction  $n_s(T)$ ) is temperature independent and  $\Delta(T)/\Delta_0$  (is well approximated with the function  $\cos^{1/2}(\pi(T/T_c)^2)$ ). In this model the superfluid fraction  $n_s(T)$  decreases with increasing temperature due to the thermal excitation of quasi-particles across the superconducting energy gap, thus reducing the number of paired electrons. For isotropic Fermi surfaces and for s-wave pairing the function  $n_s(T)$  lies significantly below the two-fluid result  $n_s(T) = 1 - (T/T_c)^4$ . However, the temperature dependence of  $n_s(T)$

is not robust and is influenced by Fermi surface anisotropy [36]. At the same time the homogeneous mixing of Cooper pairs with thermally excited quasi-particles results in a decreased gap parameter, as follows directly from the Hartree approximation to the superconducting wavefunction. The smaller gap again enhances the density of quasi-particles so that the temperature dependences of  $n_s$  and  $\Delta$  are linked in a self-consistent manner. In this context it is perhaps interesting to point out, that one can speculate that in this case there is a phase separation between normal portions (or thermions [44]) and superconducting portions which contain only Cooper pairs [15,44]. Although phase separation requires a negative interface energy between the superconducting and the normal components, a condition for which no physical reason is known to exist, the insensitivity of the gap parameter to temperature, as well as the precursor edge above  $T_c$ , follows naturally from such a model. The transition to the superconducting state is completed at the percolation threshold. This picture has some features in common with the model by J.C. Phillips [45] based on quantum percolation of precursive local superconducting fluctuations. The difference with the above approaches is that the local superconducting fluctuations are tied to sample inhomogeneities, which does not require a negative superconducting/normal interface energy.

#### 4.4. Implications of the ad hoc two-fluid model

Why works an ad hoc two-fluid model with a temperature-independent gap so well compared to weak- or strong-coupling BCS theory? First we observe that the good correspondence between fig. 13(b) and fig. 6 may be misleading, as a priori there is no reason why the spectral shape should look similar to BCS theory as soon as one drops the temperature dependence of the gap in BCS theory and the BCS prediction for the  $2\Delta/k_B T_c$  ratio. A logical alternative is to consider strong-coupling Eliashberg theory, which is at least capable of producing a large  $2\Delta/k_B T_c$  ratio. If applied to the case of  $T=0$  there is no direct problem with the use of such an approach, but the difficulty at finite temperature is again that this theory predicts a superconducting gap that vanishes at  $T_c$ , albeit the descent near  $T_c$  is steeper than in the weak-coupling limit. In the mean-field implementation of

Eliashberg, strong-coupling theories do however not provide the gap-like precursor above  $T_c$ .

The presence of this precursor however hints in another direction. One can speculate on a scenario where the phase transition takes place at a temperature much lower than the temperature where the gap would normally close. The layered two-dimensional nature of the material could play a central role here. Rather than by breaking up Cooper pairs the superconducting ground state would be destroyed through thermal excitation of e.g. collective phase/density oscillations [43], local pairs [46] or pairing bag excitations [48]. Through their very nature the above-mentioned excitations destroy phase coherence without necessarily breaking up pairs. It remains to be seen whether the precursor above the transition temperature is better described by non-gaussian superconducting fluctuations (macroscopic fluctuations) or as metastable local pairs participating in a mixture of local pairs and unpaired particles (microscopic fluctuations). The pairing fluctuations are intermediated by some interaction mechanism of either elastic or electronic nature. Historically the term bipolaron is reserved for the former case. In the theoretical approaches of Emin [40] and de Jongh [41] above  $T_c$  all charge carriers are already bound in pairs. The superconducting transition is then a Bose condensation of these pairs. The edge at 50 meV observed with the various spectroscopies would then correspond to twice the energy required to remove a charge carrier (electron or hole) from the potential well in which it is self-trapped [40] as has been shown by Anderson [42] for the negative- $U$  Hubbard model in amorphous semiconductors. The only requirement is that the particles are paired; it is not necessary to have a superfluid condensate. A model of Bose condensation agrees with two of our observations: (1) the persistence of a gap above  $T_c$  and (2) the two-fluid-like behaviour of the superfluid density. However, it does not agree with the observation that the absorption edge “fills in” with the characteristic temperature dependence displayed in fig. 12. As the number of paired charge carriers does not change in the bipolaron model one rather expects the height of the edge to be more or less constant, only changing due to the temperature dependence of the scattering rate. In photo-electron spectroscopy no states should be observed below this

gap at all temperatures below and above  $T_c$ , but in infrared spectroscopy an additional Drude term grows on increasing the temperature due to the damped motion of non-condensed bipolarons. The failure of the pure Bose-condensation model does not come as a big surprise if we consider the estimated size of the bipolarons relative to the interparticle distance. The size of a bipolaron is of the order of a few lattice spacings. Even if one assumes that the bipolarons are localized within a single unit cell this would be of the same order of magnitude of the average spacing between holes at intermediate and high doping levels. Only in the limit where the local pairs are true point bosons they obey boson commutation rules. Otherwise, such as in the present case, one obtains large corrections to the commutation rules [43]. The superconducting ground state in such a case is very similar to a Bose condensate of slightly overlapping Cooper pairs. Without overlap the normal state would be a gas of free bipolarons. The fact that there is some spatial overlap has the effect of decomposing at least part of the pairs in the normal state. In a usual BCS superconductor (strong and weak coupling), where the spatial overlap between Cooper pairs is large, this decomposition of the paired electrons is the dominant mechanism which drives the system normal at  $T_c$ . The situation in the high- $T_c$  superconductors appears to be intermediate between the two limits of point-like bosons and strongly overlapping Cooper pairs, which is perhaps the key to understanding the phenomenology discussed in this paper. A consequence of breaking part of the local pairs above  $T_c$  would be that the “normal” state becomes a mixture of paired and unpaired charge carriers.

A possibility related to Bose condensation of bipolarons is that above  $T_c$  only part of the charge carriers are bound into pairs. This situation has among others been modeled by Micnas, Ranninger and Robaszkiewicz [46], and Schmitt-Rink [49]. The models can in principle account for the linear temperature dependence of the resistivity and various other properties of cuprate superconductors. A large ratio of  $2\Delta/k_B T_c$  follows from this theory if the number of paired charge carriers is sufficiently large. In the model of Micnas et al. [46], and recent model by Bar-Yam [47] the local pairs and unpaired charge carriers exist in separate bands and the distribution

of carrier over the two bands is determined by the energy of the bands. Pairing of the wide-band carriers occurs as a consequence of hybridisation with the Bose-condensed local pairs in the narrow band. A phase transition of the type expressed in our experimental fig. 12 requires a temperature dependent cross-over of unpaired charge carriers to Bose-condensed pairs between 90 K and 50 K. The temperature dependence of the optical response function using the models has not yet been calculated.

## 5. Conclusions

We report on detailed measurements of the infrared reflectivity of  $Y_1Ba_2Cu_3O_{7-x}$  films prepared with pulsed in situ laser deposition. We observe critical behaviour at the superconducting transition temperature in the feature of about  $8k_B T_c$  previously attributed to the in-plane  $2\Delta$  by Schlesinger et al. Our data show in unprecedented detail that the feature does not shift with temperature, but instead gradually fills in as  $T$  approaches  $T_c$  from below, where it saturates. From comparison with theoretical spectra we show that the observed thermal behaviour does not agree with standard BCS theory, but a good fit is obtained if we assume that the superconducting transition is characterized by a second order transition in the *density* of a BCS-like superconducting component with a temperature independent gap. Above the superconducting transition temperature a precursor is observed at  $400\text{ cm}^{-1}$ , the same position as the gap-related feature below  $T_c$ . The various spectral features agree very well with earlier infrared reflectivity data, with high-resolution energy-loss spectroscopy and with infrared transmission data. The observed temperature dependence of the superfluid component agrees with observations of the London penetration depth, and the notion of two-fluid behaviour is in good agreement with the observed absence of a Hebel-Slichter peak in the Korringa relaxation rate. The finding of a precursor gap above  $T_c$  hints in the direction of the presence of local pair fluctuations or bipolarons in addition to non-paired charge carriers above  $T_c$ .

## Acknowledgements

One of us (DvdM) likes to thank K. von Klitzing for hospitality and financial support during his stay at the Max-Planck-Institut. The authors have benefited from stimulating discussions with L. Genzel, M. Cardona, R. Micnas, D. Emin, C. Thomson, B. Friedl, A.B. Kaiser and M. Bauer during the preparation of this work. We like to thank R.K. Kremer for performing susceptibility measurements, G.E. Rietveld for resistivity measurements and G. Mertens and B. Leibold for technical assistance.

## References

- [1] J.G. Bednorz and K.A. Müller, *Z. Phys. B* 64 (1986) 189; M.K. Wu, J.R. Ashburn, C.J. Torng, P.H. Hor, R.L. Meng, L. Gao, Z.J. Huang, Y.Q. Wang and C.W. Chu, *Phys. Rev. Lett.* 58 (1987) 908.
- [2] L.C. Hebel and C.P. Slichter, *Phys. Rev.* 113 (1959) 1504.
- [3] W.W. Warren Jr., R.E. Walstedt, G.F. Brenner, R.J. Cava, R. Tycko, R.F. Bell and G. Dabbagh, *Phys. Rev. Lett.* 62 (1989) 119.
- [4] A.D. Wieck, E. Batke, U. Merkt, D. Walker and A. Gold, *Solid State Commun.* 69 (1989) 553.
- [5] Z. Schlesinger, R.T. Collins, F. Holtzberg, C. Feild and A. Gupta, *Phys. Rev. B* 41 (1990) 11237; R.T. Collins, Z. Schlesinger, F. Holtzberg and C. Field, *Phys. Rev. Lett.* 63 (1989) 422.
- [6] J. Orenstein, G.A. Thomas, A.J. Millis, S.L. Cooper, D.H. Rapkine, T. Timusk, L.F. Schneemeyer and J.V. Waszczak, *Phys. Rev. B* 42 (1990) 6342.
- [7] J. Schützmann, W. Ose, J. Keller, K.F. Renk, B. Roas, L. Schultz and G. Saemann-Ischenko, *Europhys. Lett.* 8 (1989) 679.
- [8] T. Timusk, S.L. Herr, K. Kamaras, C.D. Porter, D.B. Tanner, D.A. Bonn, J.D. Garrett, C.V. Stager, J.E. Greedan and M. Reedyk, *Phys. Rev. B* 38 (1988) 6683; K. Kamaras, S.L. Herr, C.D. Porter, N. Tache, D.B. Tanner, S. Etemad, T. Venketasan, E. Chase, A. Inam, X.D. Wu, M.S. Hegde and B. Dutta, *Phys. Rev. Lett.* 64 (1990) 84.
- [9] J. Demuth, B.N.J. Persson, F. Holtzberg and C.V. Chandrasekhar, *Phys. Rev. Lett.* 64 (1990) 603; B.N.J. Persson and J.E. Demuth, *Phys. Rev. B* 42 (1990) 8057.
- [10] J.M. Imer, F. Patthey, B. Dardel, W.D. Schneider, Y. Baer, Y. Petroff and A. Zettl, *Phys. Rev. Lett.* 62 (1989) 336.
- [11] J. Geerk, X.X. Xi and G. Linker, *Z. Phys. B* 73 (1988) 329; A. Kussmaul, J.S. Moodera, G.M. Roesler and P.M. Tedrow, *Phys. Rev. B* 41 (1990) 842; J.R. Kirtley, *Int. J. of Mod. Phys. B* 4 (1990) 201.
- [12] B. Friedl, C. Thomson and M. Cardona, *Phys. Rev. Lett.* 65 (1990) 915.
- [13] L. Genzel, A. Wittlin, J. Kuhl, H. Mattausch, W. Bauhofer and A. Simon, *Solid State Commun.*, 63 (1987) 843; A. Wittlin, L. Genzel, M. Cardona, M. Bauer, W. König, E. Garcia, M. Barahona and M.V. Cabanas, *Phys. Rev. B* 37 (1988) 652; E. Seider, M. Bauer, L. Genzel, P. Wyder, A. Jansen and C. Richter, *Solid State Comm.* 72 (1989) 85; G.A. Thomas, J. Orenstein, D.H. Rapkine, M. Capii, A.J. Millis, R.N. Bhatt, L.F. Schneemeyer and J.V. Waszczak, *Phys. Rev. Lett.* 61 (1988) 1313.
- [14] D. van der Marel, M. Bauer, E.H. Brandt, H.-U. Habermeier, D. Heitmann, W. König and A. Wittlin, *Phys. Rev. B* 43 (1991) 8606; R.T. Collins, Z. Schlesinger, F. Holzberg, C. Field, U. Welp, G.W. Crabtree, J.Z. Liu and Y. Fang, *Phys. Rev. B* 43 (1991) 8701.
- [15] D. van der Marel, *Proc. XIV. Int. School on Theoretical Physics, Strongly Correlated Systems and High- $T_c$  Superconductivity*, Szczyrk, Poland (15–22 Sept. 1990) (World Scientific, Singapore) to be published.
- [16] L. Coffey, *Phys. Rev. Lett.* 64 (1990) 1071.
- [17] B.W. Statt, *Phys. Rev. B* 42 (1990) 6805.
- [18] H.-U. Habermeier and G. Mertens, *Physica C* 162–164 (1989) 601.
- [19] J.C. Galzerani and R.S. Katiyar, *Solid State Commun.* 41 (1982) 515.
- [20] B. Koch, H.P. Geserich and T.H. Wolf, *Solid State Commun.* bf 71 (1989) 495; Z. Schlesinger, R.T. Collins, F. Holzberg, C. Feild, S.H. Blanton, U. Welp, G.W. Crabtree, Y. Fang and J.Z. Liu, *Phys. Rev. Lett.* 65 (1990) 801.
- [21] J.W. Loram, K.A. Mirza and P.F. Freeman, *Physica C* 171 (1990) 243.
- [22] N.E. Phillips, R.A. Fisher, J.E. Gordon, S. Kim, A.M. Stacy, M.K. Crawford and E.M. McCarron, *Phys. Rev. Lett.* 65 (1990) 357.
- [23] B. Batlogg, *High Temperature Superconductivity—The Los Alamos Symposium 1989*, eds. K. Bedell, D. Coffey, D. Meltzer, D. Pines and J.R. Schrieffer (Addison-Wesley, Reading, MA, 1990) p. 37.
- [24] M. Affronte, D. Pavuna, M. Francois, F. Licci, T. Besagni and S. Cattani, *Physica C* 162–164 (1989) 1007.
- [25] D.B. Romero, G.L. Carr, D.B. Tanner, L. Forro, D. Mandrus, L. Mihaly and G.P. Williams, preprint; L. Forro, G.L. Carr, G.P. Williams, D. Mandrus and L. Mihaly, *Phys. Rev. Lett.* 65 (1990) 1941.
- [26] A.B. Kaiser and C. Uher, in: *Studies of High Temperature superconductors*, vol. 7, ed. A.V. Narlikar (Nova, New York, 1990).
- [27] A.B. Kaiser, private communication.
- [28] T. Timusk and D.B. Tanner, *Physica C*, 169 (1990) 425.
- [29] N.E. Bickers, D.J. Scalapino, R.T. Collins and Z. Schlesinger, *Phys. Rev. B* 42 (1990) 67.
- [30] W. Lee, D. Rainer, and W. Zimmermann, *Physica C* 159, (1989) 535.
- [31] P.B. Allen and D. Rainer, *Nature* 349 (1991) 396.

- [32] Y.H. Kim, A.J. Heeger, L. Acedo, G. Stucky and F. Wudl, *Phys. Rev. B* 36 (1987) 7252.  
Y.H. Kim, C.M. Foster, A.J. Heeger, S. Cox and G. Stucky, *Phys. Rev. B* 38 (1988) 6478;  
C. Talliani, R. Zamboni, G. Ruani, F.C. Maticcotta and K.I. Pokjodnya, *Solid State Commun.* 66. (1987) 736.
- [33] The theory for the electromagnetic properties of superconducting alloys has been formulated by A.A. Abrikosov, L.P. Gorbov, and I.E. Dzyaloshinski in: *Methods of quantum field theory in statistical physics*, rev. English edition, ed. R.A. Silverman (Prentice-Hall Englewood Cliffs, NJ). See especially pp. 334–341. A reformulation of the problem can be found in the Master's thesis of W. Zimmermann, University of Bayreuth (1983). We used a Fortran routine based on the latter equations, which was published in: E.H. Brandt, M. Bauer, E. Seider, and L. Genzel, *Proc. USSR-FRG Bilateral Seminar, Investigation of the High Temperature Superconductors—Modern Spectroscopic and Microscopic Methods*”, Tallinn, USSR (1989).
- [34] D.C. Mattis and J. Bardeen, *Phys. Rev.* 111 (1958) 412.
- [35] L. Leplace, *Phys. Rev. B* 27 (1983) 1911.
- [36] T. Schneider and M.P. Sørensen, *Z. Phys. B* 81 (1990) 3.
- [37] V.Z. Kresin and S.A. Wolf, *Physica C* 169 (1990) 476.
- [38] M. Bauer, Ph. D. Thesis, University of Tübingen (1990) unpublished.
- [39] C.J. Gorter and H.B.G. Casimir, *Phys. Z.* 35 (1934) 963.
- [40] D. Emin and M.S. Hillery, *Phys. Rev. B* 39 (1989) 6575.
- [41] L.J. de Jongh, *Physica C* 152 (1988) 171.
- [42] P.W. Anderson, *Phys. Rev. Lett.* 34 (1975) 953.
- [43] D. van der Marel, *Physica C* 165 (1990) 35.
- [44] E. Pakulis, *Phys. Rev. B* 42 (1990) 10746.
- [45] J.C. Phillips, *Phys. Rev. B* 42 (1990) 8623, and references therein.
- [46] R. Micnas, J. Ranninger and S. Robaszkiewicz, *Rev. Mod. Phys.* 62 (1990) 113, and references therein.
- [47] Y. Bar-Yam, *Phys. Rev. B* 43 (1991) 359; *ibid.* 43 (1991) 2601.
- [48] A.R. Bishop, P.S. Lomdahl, J.R. Schrieffer and S.A. Trugman, *Phys. Rev. Lett.* 61 (1988) 2709.
- [49] S. Schmitt-Rink, C.M. Varma and A.E. Ruckenstein, *Phys. Rev. Lett.* 63 (1989) 445.